

## Transforming graphite to nanoscale diamonds by a femtosecond laser pulse

R. Nüske, A. Jurgilaitis, H. Enquist, M. Harb, Y. Fang et al.

Citation: *Appl. Phys. Lett.* **100**, 043102 (2012); doi: 10.1063/1.3678190

View online: <http://dx.doi.org/10.1063/1.3678190>

View Table of Contents: <http://apl.aip.org/resource/1/APPLAB/v100/i4>

Published by the [American Institute of Physics](http://www.aip.org).

---

### Related Articles

Magnetic-field-induced martensitic transformation in MnNiAl:Co alloys

*Appl. Phys. Lett.* **100**, 152401 (2012)

Two-dimensional order-disorder transition of argon monolayer adsorbed on graphitized carbon black: Kinetic Monte Carlo method

*J. Chem. Phys.* **136**, 134702 (2012)

Piezoelectric properties and temperature stability of Mn-doped Pb(Mg<sub>1/3</sub>Nb<sub>2/3</sub>)-PbZrO<sub>3</sub>-PbTiO<sub>3</sub> textured ceramics

*Appl. Phys. Lett.* **100**, 132908 (2012)

Phase transitions between the rotator phases of paraffin investigated using silicon microcantilevers

*J. Chem. Phys.* **136**, 104903 (2012)

Structural and magnetic phase transition of mixed olivines Li<sub>x</sub>Fe<sub>1-y</sub>Ni<sub>y</sub>PO<sub>4</sub> by lithium deintercalation

*J. Appl. Phys.* **111**, 07D722 (2012)

---

### Additional information on *Appl. Phys. Lett.*

Journal Homepage: <http://apl.aip.org/>

Journal Information: [http://apl.aip.org/about/about\\_the\\_journal](http://apl.aip.org/about/about_the_journal)

Top downloads: [http://apl.aip.org/features/most\\_downloaded](http://apl.aip.org/features/most_downloaded)

Information for Authors: <http://apl.aip.org/authors>

## ADVERTISEMENT



**Goodfellow**  
metals • ceramics • polymers • composites  
70,000 products  
450 different materials  
**small quantities fast**

[www.goodfellowusa.com](http://www.goodfellowusa.com)

## Transforming graphite to nanoscale diamonds by a femtosecond laser pulse

R. Nüske,<sup>1</sup> A. Jurgilaitis,<sup>1</sup> H. Enquist,<sup>1</sup> M. Harb,<sup>1</sup> Y. Fang,<sup>2,3</sup> U. Håkanson,<sup>2,3</sup> and J. Larsson<sup>1,a)</sup>

<sup>1</sup>Atomic Physics Division, Department of Physics, Lund University, P.O. Box 118, SE-221 00 Lund, Sweden

<sup>2</sup>Division of Solid State Physics/The Nanometer Structure Consortium at Lund University (nmC@LU), P.O. Box 118, S-221 00 Lund, Sweden

<sup>3</sup>Beijing National Laboratory for Condensed Matter Physics, Institute of Physics, Chinese Academy of Sciences, P.O. Box 603-146, 100190 Beijing, China

(Received 4 December 2011; accepted 30 December 2011; published online 23 January 2012)

Formation of cubic diamond from graphite following irradiation by a single, intense, ultra-short laser pulse has been observed. Highly oriented pyrolytic graphite (HOPG) samples were irradiated by a 100 fs pulse with a center wavelength of 800 nm. Following laser exposure, the HOPG samples were studied using Raman spectroscopy of the sample surface. In the laser-irradiated areas, nanoscale cubic diamond crystals have been formed. The exposed areas were also studied using grazing incidence x-ray powder diffraction showing a restacking of planes from hexagonal graphite to rhombohedral graphite. © 2012 American Institute of Physics. [doi:10.1063/1.3678190]

The types of bonds in carbon-based materials range from the extremely strong  $sp^3$  bonds in diamond to the weak van der Waals bonds in graphite. As a result of the many types of bonds, a large variety of natural and man-made allotropes of carbon exist. Finding controlled pathways between these allotropes and, in particular, being able to transform graphite to diamond is a subject that has fascinated scientists and engineers for a century. Artificially created diamond was first reported on by Bundy *et al.* in 1955.<sup>1</sup> In their seminal work, they synthesized diamond by subjecting graphite to high temperature and pressure. Today, CVD grown diamonds rival the quality of natural diamonds, but the topic of transforming the material remains intriguing due to the lack of understanding of the key mechanisms underlying such phase transformations. There are also emerging technical applications for nano-diamonds, which were recently reviewed by Baidakova and Vul'.<sup>2</sup> The wide range of applications has inspired many novel methods for syntheses including high-pressure, high-temperature transformation during detonation of carbon-based explosives,<sup>3</sup> charged particle beam bombardment of graphite onions or graphite,<sup>4,5</sup> and pulsed-laser induced interfacial reaction (PLIIR) in liquids.<sup>6</sup> Yang *et al.* reported on the synthesis of nano-diamond particles consisting of both hexagonal and cubic diamond from hexagonal graphite using PLIIR with rhombohedral graphite as an intermediate.<sup>6,7</sup> So far, electron and ion bombardment of graphite<sup>4,5</sup> has proved to give an unprecedented control of size and position of the nano-diamonds, making it possible to write patterns on a surface.

The interaction of short laser pulses with graphite has been studied over the last decade in order to understand a range of processes<sup>8</sup> including laser ablation of graphite to isolate graphene.<sup>9</sup> It has also been suggested that hexagonal diamond can be created by laser-irradiation of highly oriented pyrolytic graphite (HOPG).<sup>10</sup> Work related to direct light-actuated transformation of graphite to diamond on the

surface has been carried out by Raman *et al.* who reported on transient  $sp^3$  bonded structures in laser excited graphite<sup>11</sup> and Kanasaki *et al.* who observed  $sp^3$  bonded structures on graphite with transmission electron microscopy following exposure by approximately  $10^4$  pulses.<sup>12</sup> Liu *et al.* have reported a laser-based method to write diamond patterns on graphite with  $\mu\text{m}$  precision.<sup>13</sup> This method has the potential to be a widely applicable manufacturing technique of functional nanopatterns.

In the present experiment, we irradiated HOPG with short laser pulses and created nano-diamonds that are visible in Raman spectroscopy measurements. This opens a new path to making diamond patterns on graphite with  $\mu\text{m}$  precision. We also observed laser-driven restacking of hexagonal graphite to rhombohedral graphite using grazing-incidence x-ray diffraction.

The sample used in this study was a  $12 \times 12 \times 2 \text{ mm}^3$ , ZYA grade HOPG substrate with a mosaic spread of  $0.4^\circ$ . The sample was irradiated by a single 100 fs laser pulse from a Ti:Sapphire system, with wavelength centered around 800 nm. The incident fluence was  $90 \text{ J/cm}^2$ , which resulted in visible damage of the HOPG. Each individual laser spot size was  $0.15 \times 0.15 \text{ mm}^2$ . An array of single laser-pulse irradiated spots with a size of  $0.15 \times 3.0 \text{ mm}$  was created. The separation between individual spots was 0.25 mm.

After laser irradiation, the Raman spectrum of the sample was analyzed using a fiber-coupled Raman microscope system to study the phonon characteristics of the irradiated sample. The Raman system is equipped with an imaging CCD and a motorized stage allowing for simple identification of the laser-irradiated spots. Raman spectra were obtained in a backscattering configuration using a  $100\times$  objective (NA 0.8) and a 632.8 nm HeNe laser ( $\sim 2 \text{ mW}$  at the sample). The system provides an overall spatial resolution of  $1 \mu\text{m}$  and a probing depth of about 100 nm.<sup>14</sup>

The crystal structure was analyzed using grazing incidence x-ray powder diffraction performed at beamline D611 at the MAX-laboratory synchrotron radiation facility in Lund<sup>15</sup> using a 2D detector.<sup>16</sup> The x-ray spot size on the

<sup>a)</sup>Author to whom correspondence should be addressed. Electronic mail: jorgen.larsson@fysik.lth.se.

sample was  $0.2 \times 2.5 \text{ mm}^2$  at the incidence angle of  $0.8^\circ$  used in the experiment. This x-ray footprint is comparable to the spatial extent of the array of single laser-pulse irradiated spots. The photon energy of the x-rays was 9 keV and the bandwidth  $\Delta E/E = 0.1\%$ . X-rays incident on a phosphor screen were imaged onto a CCD camera. The images were recorded and analyzed in order to produce the powder patterns. The set-up was calibrated with silicon powder. The set-up allowed for coverage of a q-range from 2.9 to  $4.4 \text{ \AA}^{-1}$  with a q-resolution of  $0.02 \text{ \AA}^{-1}$ .

Raman spectroscopy provides high spatial resolution and surface sensitivity. An image of the laser-irradiated sample from the Raman microscope is shown in Fig. 1. The Raman spectra from both pristine and laser-irradiated HOPG are shown in Fig. 2. Within the laser-exposed area, the measured Raman spectra vary locally. A striking feature in the Raman spectrum obtained at position B is the peak at  $1332 \text{ cm}^{-1}$ , which is the characteristic Raman peak for the  $T_{2g}$  phonon mode in cubic diamond.<sup>17</sup> This clearly shows formation of nano-diamonds in the laser-exposed area. The line width of the measured diamond peak is  $20 \text{ cm}^{-1}$ . The feature at  $1580 \text{ cm}^{-1}$  can be identified as the  $E_{2g}$  mode of graphite and is present in all spectra.<sup>18</sup> In laser irradiated areas we find a broad feature seen in the Raman spectrum obtained at position B at  $1360 \text{ cm}^{-1}$ , which originates from the graphite  $A_{1g}$  mode. This mode becomes Raman active due to laser-induced disorder in the graphite structure.<sup>19</sup>

In order to obtain additional insights on the nano-diamond formation, we investigated our samples using x-ray powder diffraction. The result is seen in Fig. 3 where we show powder diffraction data from laser-exposed areas as well as from areas with pristine HOPG. It is evident that all peaks can be identified as reflections from either hexagonal or rhombohedral graphite. The rhombohedral modification of graphite can be found only after the laser irradiation. The structure of rhombohedral graphite (ABCA) can be understood as an extended stacking fault of the hexagonal configuration (ABAB) and is known to be generated when hexagonal graphite is deformed mechanically. What is clear

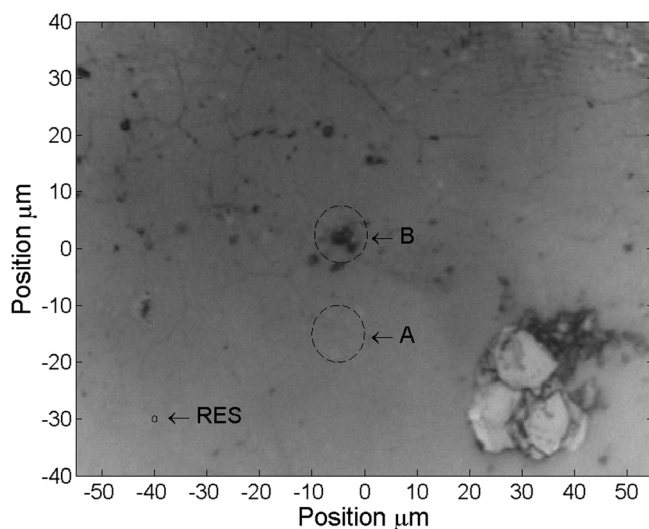


FIG. 1. Image of the laser-irradiated graphite sample taken in the Raman microscope. Circles A and B show where measurements were carried out. The small circle marked “RES” indicates the resolution of the instrument.

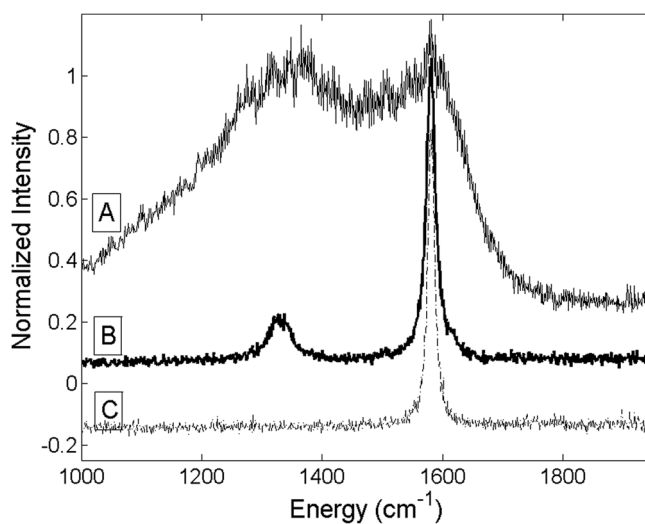


FIG. 2. Raman spectra of HOPG after femtosecond laser irradiation (A) and (B) and pristine HOPG (C).

is that a single laser pulse can restack the graphite. No reflections from hexagonal or cubic diamond are present in the powder diffraction data. These findings are consistent with the work of Wang and Yang<sup>7</sup> who used the PLIIR method for graphite to diamond conversion.

The Raman data clearly shows the presence of cubic diamond in the irradiated sample. Furthermore, we found a correlation between the presence of cubic diamond and the areas that appear black in the microscope image. The resolution associated with the focal spot in the Raman microscope is about  $1 \mu\text{m}$ . The discolored areas were  $1\text{--}10 \mu\text{m}$  in size, showing that diamond-dense regions of a few microns in size exist. Yoshikawa *et al.* reported on the effect of crystal size on the line-width of Raman spectra of cubic diamond.<sup>20</sup> According to this model, which accounts for homogeneous broadening of the Raman line due to phonon confinement and damping, the individual cubic diamond crystals found in this work are at least 8 nm in size. This is a minimum value which does not take into account that other broadening mechanisms such as strain may be present.

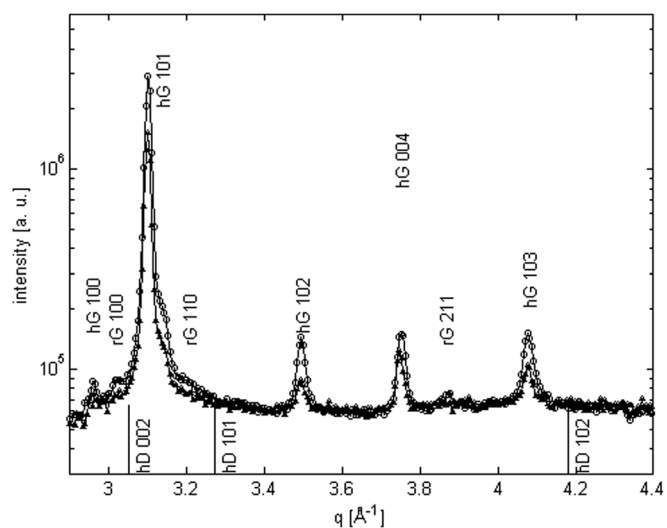


FIG. 3. Grazing incidence powder x-ray diffraction.  $\Delta, \circ$  are experimental data before and after laser exposure; hG, rG, hD, and cD denote the positions of hexagonal graphite, rhombohedral graphite, hexagonal diamond, and cubic diamond, respectively.

The result of our powder diffraction measurements is in disagreement with a recent study by Sano *et al.*<sup>10</sup> in which the authors claim to see powder diffraction pattern from hexagonal diamond from laser-excited graphite, but no evidence of cubic diamond. Since we did not see any evidence of neither cubic nor hexagonal diamond, we reinvestigated their data. The authors showed x-ray powder diffraction data covering a  $q$ -range range of 2.8–3.6 Å<sup>-1</sup> with a resolution of 0.03 Å<sup>-1</sup>. Table I summarizes results obtained from Ref. 10 and this study together with values for hexagonal<sup>21</sup> and cubic diamonds and hexagonal and rhombohedral graphites.<sup>22</sup> A comparison shows that the data presented in the work of Sano *et al.* is better explained with the hexagonal and rhombohedral modification of graphite. In particular, the 100 reflection of hexagonal diamond at 2.87 Å is not present in their data. Furthermore, the peaks at 3.01 and 3.20 Å are better matched with reflections from rhombohedral graphite. The lack of x-ray signal from diamond in either study is due to the small total area covered with cubic diamonds. Similarly nanodiamonds created by PLIIR described by Wang and Yang<sup>7</sup> were observed with electron diffraction whereas it was not possible to observe them with x-ray powder diffraction.

We discuss three potential mechanisms for the formation of diamond. The first is similar to the mechanism in a shock-wave experiment. Within a few picoseconds after laser excitation, the temperature of the material rises to the melting level. When the topmost layer is molten, the graphite starts to expand towards the density of liquid carbon. As this occurs, a pressure is formed at the boundary between the solid and liquid phases of the material, launching a strain wave into the material.<sup>23</sup> Since the density of liquid carbon (1.6 g/cm<sup>3</sup> (Ref. 24)) differs significantly from that of graphite (2.26 g/cm<sup>3</sup>), the shock wave amplitude is large. The amplitude can be calculated by solving the elastic equations, similar to Thomsen *et al.*,<sup>25</sup> if the density, compressibility, and speed of sound are known for the solid and liquid phases. In our discussion aimed at estimating the stress in the solid, we assume a constant bulk modulus and neglect the influence of the change of density. The compressibility of liquid carbon is  $6.4 \times 10^{-12} \text{ Pa}^{-1}$ ,<sup>24</sup> corresponding to a bulk modulus of  $K = 150 \text{ GPa}$ . The density mismatch between the solid and liquid corresponds to a strain  $\eta = (\rho_{\text{solid}} - \rho_{\text{liquid}})/\rho_{\text{liquid}} = 41\%$  in the liquid. The stress at the solid-liquid boundary is then

$$s = \frac{K}{2} \eta (1 + R), \quad (1)$$

$R$  is the reflectivity of the stress wave at the boundary given by

$$R = \frac{\rho_{\text{solid}} v_{\text{solid}} - \rho_{\text{liq}} v_{\text{liquid}}}{\rho_{\text{solid}} v_{\text{solid}} + \rho_{\text{liq}} v_{\text{liquid}}}. \quad (2)$$

The speed of sound in the liquid is given by  $v_{\text{liquid}} = (K/\rho_{\text{liquid}})^{1/2}$  and along the  $c$ -axis in the solid by  $v_{\text{solid}} = (C_{33}/\rho_{\text{solid}})^{1/2}$ , where  $C_{33}$  is the relevant elastic constant. At early times the newly formed liquid is still at the solid density, and therefore the solid density is used in both cases. This yields  $v_{\text{liquid}} = 8260 \text{ m/s}$ ,  $v_{\text{solid}} = 4000 \text{ m/s}$ , and a reflectivity of  $R = -35\%$ . The factor 2 in Eq. (1) originates from the fact that two counter-propagating waves are created. The sum of the static strain and the two counter propagating waves must be zero at the time of generation to fulfill the initial condition of zero strain. The boundary condition requires the stress to be equal on the two sides of the solid-liquid boundary.<sup>25</sup> When evaluating the equation above we find that the amplitude of the stress wave in graphite is 20 GPa. Near the molten material, the temperature of the solid equals the melting temperature of graphite  $T = 3900 \text{ K}$ . Under traditional shock experiments the transformation has been shown to be martensitic below 2000 K and hexagonal diamond is created. Cubic diamond is believed to be created from hexagonal diamond. At temperatures above 4000 K only cubic diamond is formed.<sup>26</sup> It should be noted that in our study, the high pressure would last only for 5-10 ps. In our work, there is no indication of hexagonal diamond which would manifest itself as a Raman peak between 1319 and 1326 cm<sup>-1</sup>.<sup>27</sup>

A second mechanism for the transformation is a coherent phonon motion. In the study by Kanasaki *et al.*<sup>12</sup> the formation of  $sp^3$  bonds at the surface of the HOPG sample was induced using much lower laser fluence. The mechanism in this case does not need to be pressure driven. The authors speculate on a restacking to AAA graphite followed by buckling of planes and formation of  $sp^3$  bonds. Such restacking has been predicted by tight binding molecular dynamics (TBMD) calculations.<sup>28</sup> These calculations did not show any diamond formation. It was however suggested in Ref. 7 that the observed rhombohedral graphite is an intermediate to cubic diamond. The findings were supported by analyzing the orientation of the formed diamonds compared to the orientation of the graphite.

A third mechanism is that diamonds are formed during rapid quenching. Small diamond structures were found following irradiation of ms laser pulses in a high-pressure He atmosphere.<sup>29</sup> The Raman peaks observed in Ref. 29 had a significantly larger width ( $\text{FWHM} = 60 \text{ cm}^{-1}$ ) indicating smaller size or more severe strain compared to the present work.

In conclusion we find that static measurement cannot distinguish the three mechanisms discussed above. A clear way of identifying the relevant one is to carry out an experiment showing the birth of a diamond following laser excitation. The time-scale for the generation is clearly different in the three cases, since a coherent transformation takes place in less than 1 ps, a pressure-driven transition will occur in a

TABLE I. Powder diffraction data from this work and Ref. 10 compared to peak positions for hexagonal graphite (hG), rhombohedral graphite (rG),<sup>21</sup> and hexagonal diamond (hD).<sup>22</sup>

Ref. 10	Powder x-ray diffraction peak position $q$ (Å <sup>-1</sup> )				
	This work	hG	hD	rG	cD
2.95	2.94	2.95	2.87		
3.01	3.01		3.05	3.02	3.05
3.09	3.10	3.10			
3.20	3.18		3.27	3.21	
3.50	3.49	3.50			
	3.75	3.75		3.75	
	4.07	4.08	4.18	3.87	4.98

few ps and diamond formation due to quenching takes place during cooling of the liquid which takes about 100 ps.

The authors would like to thank the Swedish Research Council (VR), the Knut and Alice Wallenberg Foundation, the Crafoord Foundation and Stiftelsen Olle Engkvist byggmästare for financial support. M.H. acknowledges financial support from the Natural Sciences and Engineering Research Council of Canada.

- <sup>1</sup>F. P. Bundy, H. T. Hall, and H. M. Strong, *Nature* **176**, 51 (1955).
- <sup>2</sup>M. Baidakova and A. Vul', *J. Phys. D: Appl. Phys.* **40**, 6300 (2007).
- <sup>3</sup>M. Van Thiel and F. H. Ree, *J. Appl. Phys.* **62**, 1761 (1987).
- <sup>4</sup>F. Banhart and P. M. Ajayan, *Nature* **382**, 433 (1996).
- <sup>5</sup>A. Dunlop, G. Jaskierowicz, P. M. Ossi, and S. Della-Negra, *Phys. Rev B* **76**, 155403 (2007).
- <sup>6</sup>G. W. Yang, J. B. Wang, and Q. X. Liu, *J. Phys.: Cond. Mat.* **10**, 7923 (1998).
- <sup>7</sup>G. W. Yang and J. B. Wang, *Appl. Phys. A* **72**, 475 (2001).
- <sup>8</sup>M. D. Shirk and P. A. Molian, *Carbon* **39**, 1183 (2001).
- <sup>9</sup>M. Lenner, A. Kaplan, Ch. Huchon, and R. E. Palmer, *Phys. Rev. B* **79**, 184105 (2009).
- <sup>10</sup>T. Sano, K. Takahashi, O. Sakata, M. Okoshi, N. Inoue, K. F. Kobayashi, and A. Hirose, *J. Phys.: Conf. Ser.* **165**, 012019 (2009).
- <sup>11</sup>R. K. Raman, Y. Murooka, C.-Y. Ruan, T. Yang, S. Berber, and D. Tománek, *Phys. Rev. Lett.* **101**, 077401 (2008).
- <sup>12</sup>J. Kanasaki, E. Inami, K. Tanimura, H. Ohnishi, and K. Nasu, *Phys. Rev. Lett.* **102**, 087402 (2009).
- <sup>13</sup>P. Liu, C. Wang, J. Chen, N. Xu, G. W. Yang, N. Ke, and J. Xu, *J. Phys. Chem. C* **113**, 12154 (2009).
- <sup>14</sup>J. Chen, G. Conache, M. Pistol, S. Gray, M. T. Borgström, H. Xu, H. Q. Xu, L. Samuelson, and U. Håkanson, *Nano Lett.* **10**, 1280 (2010).
- <sup>15</sup>M. Harbst, T. N. Hansen, C. Caleman, W. K. Fullagar, P. Jönsson, P. Sondhauss, O. Synnergren, and J. Larsson, *Appl. Phys. A* **81**, 893 (2005).
- <sup>16</sup>R. Nüske, C. V. K. Schmising, A. Jurgilaitis, H. Enquist, H. Navirian, P. Sondhauss, and J. Larsson, *Rev. Sci. Instrum.* **81**, 013106 (2010).
- <sup>17</sup>A. C. Ferrari and J. Robertson, *Phys. Rev. B* **61**, 14095 (2000).
- <sup>18</sup>Y. Wang, D. C. Alsmeyer, and R. L. McCreery, *Chem. Mat.* **2**, 557 (1990).
- <sup>19</sup>F. Tuinstra and J. L. Koenig, *J. Chem. Phys.* **53**, 1126 (1970).
- <sup>20</sup>M. Yoshikawa, Y. Mori, M. Maegawa, G. Katagiri, H. Ishida, and A. Ishitani, *Appl. Phys. Lett.* **62**, 3114 (1993).
- <sup>21</sup>G. E. Bacon, *Acta. Crystallogr.* **3**, 320 (1950).
- <sup>22</sup>F. P. Bundy and J. S. Kasper, *J. Chem. Phys.* **46**, 3437 (1967).
- <sup>23</sup>H. Enquist, H. Navirian, T. Hansen, A. Lindenberg, P. Sondhauss, O. Synnergren, J. S. Wark, and J. Larsson, *Phys. Rev. Lett.* **98**, 225502 (2007).
- <sup>24</sup>J. Steinbeck, G. Dresselhaus, and M. S. Dresselhaus, *Int. J. Thermophys.* **11**, 789 (1990).
- <sup>25</sup>C. Thomsen, H. T. Grahm, H. J. Maris, and J. Tauc, *Phys. Rev. B* **34**, 4129 (1986).
- <sup>26</sup>D. J. Erskine and W. J. Nellis, *Nature* **349**, 317 (1991).
- <sup>27</sup>D. S. Knight and W. B. White, *J. Mater. Res.* **4**, 391 (1989).
- <sup>28</sup>M. E. Garcia, T. Dumitrica, and H. O. Jeschke, *Appl. Phys. A* **79**, 855 (2004).
- <sup>29</sup>A. Yu. Basharin, V. S. Dozhdikov, V. T. Dubinchuk, A. V. Kirillin, I. Yu. Lysenko, M. A. Turchaninov, *Tech. Phys. Lett.* **35**, 428 (2009).